Proceedings of the ASME 2024
International Design Engineering Technical Conferences and
Computers and Information in Engineering Conference
IDETC-CIE2024
August 25-28, 2024, Washington, DC

DETC2024-146393

A VISION-BASED HEALTH INSPECTION OF POWER LINE CONDUCTORS FOR THE MOBILE DAMPING ROBOT

Hyun Myung Kang, Ranhee Yoon, Oumar Barry*
Department of Mechanical Engineering
Virginia Polytechnic Institute and State University
Blacksburg, Virginia 24061

ABSTRACT

Ensuring the structural integrity of the overhead power line conductor is crucial for maintaining the safety and reliability of the electrical transmission system. Exposure to environmental hazards like moisture, dust, and Wind-Induced Vibrations (WIV) can lead to defects and corrosion in power line conductors, which are primary contributors to fatigue and shortened lifespan. Thus, this paper presents a vision-based health inspection of power line conductors for a maintenance robot. The method involves image filtering techniques such as Sobel, Scharr, and Gray-scale Variance Normalization (GVN). After filtering the image, row and column analysis is conducted to identify relevant patterns that distinguish healthy and unhealthy conductors, utilizing histograms for data representation. From the histogram data analysis, 10 features were chosen from observation. Subsequently, the collected image data is classified into either healthy or unhealthy categories through supervised machine learning models, including Random Forest (RF), Multi-Layer Perception (MLP), and Gradient Boosting (GB). The best combination of features is extracted to optimize each machine-learning models accordingly. Experimental results validated the effectiveness of our method, which has been specifically fitted for the Mobile Damping Robot (MDR), presenting its potential for enhancing power line maintenance.

Keywords: vision-based health inspection, power line conductors, image filtering, classification

*Corresponding Author (Email: obarry@vt.edu)

1 INTRODUCTION

The power line acts as a medium to transmit electricity from power generating stations to distribution stations. Thus, consistent power line inspection is key to maintaining the reliability and safety of the electric grid. When subjected to environmental hazards such as long exposure to rain, snow, dust, and other elements, the power line conductor is subjected to an increased risk of fatigue symptoms in power systems. The most common signs of fatigue include defects and corrosion. The outer layer material of power line conductors, typically aluminum, is prone to oxidation upon contact with moisture, leading to corrosion and subsequent deterioration. Figure 1 shows images depicting healthy, defective, and corroded conductors. These factors contribute to a shortened lifespan, particularly when the power line is subjected to wind-induced vibration or aeolian vibration [1].

To overcome these challenges, conventional power line inspection methods have been proposed: field surveys done by humans either by pole-climbing, foot patrolling, or inspection using a vehicle. This method, however, has numerous disadvantages such as being costly, time-consuming, and prone to human error. Additionally, with bad weather conditions and/or if the towers are located in remote places, technicians would have a difficult time assessing the health of the power lines. Alternative methods of aerial video surveillance, such as helicopters, airplanes, or unmanned aerial vehicles, have been undergoing extensive research. This method, however, presents several limitations including high costs, challenges in stabilization of cameras, and issues with capturing high-quality images of conductors from close proximity [2]. Large vehicles have difficulty approaching power line conductors closely, which affects the clarity and precision of

image capture. The level of detail in the image is essential for effectively detecting minute signs of defects and corrosion, which is a key focus of our research.

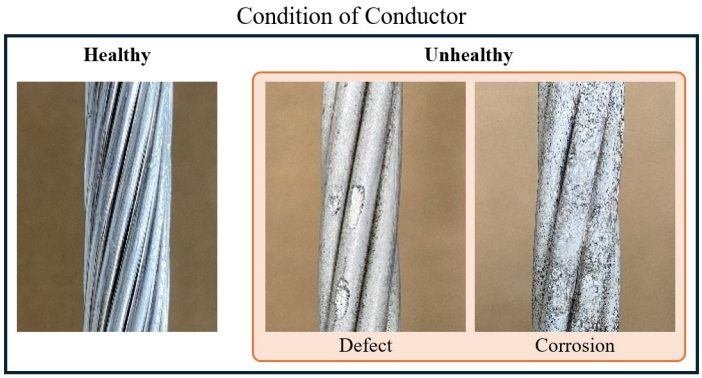

FIGURE 1: Condition classifying of a conductor.

The objective of this paper is to introduce our optimized method for vision-based detection of defects and corrosion, which are primary factors contributing to fatigue in power line conductors. We analyzed of Sobel, Scharr, and Gray-scale Variance Normalization (GVN) filters to assess their effectiveness in extracting small details of defects and corrosion while reducing noise, such as background and unwanted details on the surface of conductors. We compared the performance of each image processing technique with row and column analysis of gray-scale values of each pixel. These data are then utilized to obtain the accuracy of classification using various supervised machine learning models, including Random Forest (RF), Multi-Layer Perception (MLP), and Gradient Boosting (GB) classifiers with various combinations of identified features. It is crucial to highlight that this method has been specifically optimized for our power line maintenance robot, the Mobile Damping Robot (MDR). Through experimental validation, we have successfully demonstrated the effectiveness of our method.

This paper is structured as follows: Section 2 describes the purpose and the characteristics of the MDR. Section 3 provides a detailed analysis of the method for detecting defects and corrosion, including image filtering techniques and histogram analysis. Section 4 discusses the various supervised machine learning models used for classifying the conductors into either healthy or unhealthy categories. In Section 5, the experiment compares the effectiveness of Sobel, Scharr, and GVN image filter techniques, as well as the performance of different machine learning models and types of features extracted accordingly. Finally, sections 6 and 7 conclude with a discussion of the results and a summary of the key findings. Figure 2 illustrates the flowchart outlining the overall logic of our classification method, which will be covered in each section of the paper in order.

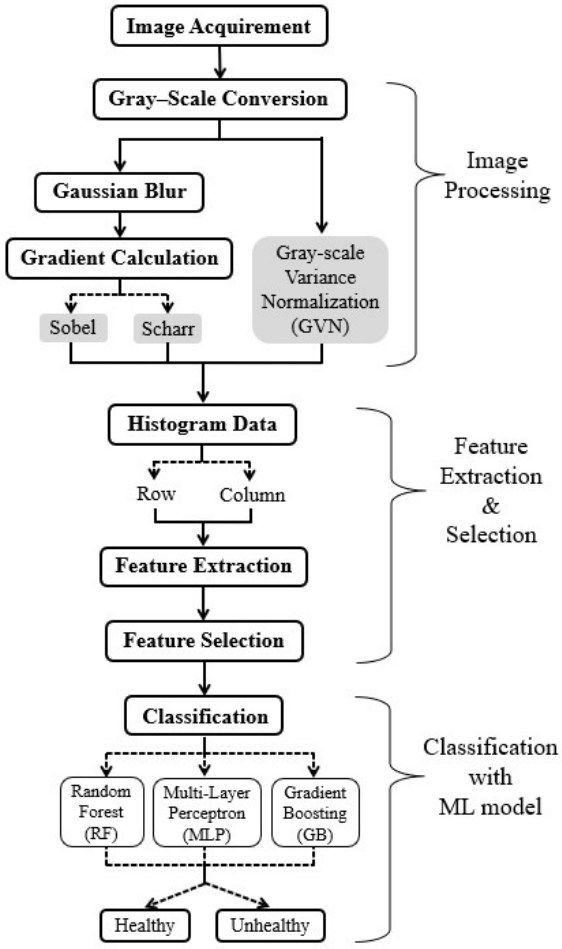

FIGURE 2: A method flowchart for healthy and unhealthy power line conductors classification.

2 POWER LINE INSPECTION MOBILE DAMPING ROBOT

To enhance accuracy and efficiency in power line inspection, significant efforts have been directed towards autonomous integration. For instance, the Kunshan Institute of Industrial Research in China introduced a climbing power line inspection robot. This robot is equipped with two legs that allows it to transverse tower obstacles like clamps and counterweights by gripping the power line conductors [3, 4]. Additionally, Unmanned Aerial Vehicles (UAV) have become increasingly popular for power line inspection due to their cost-effectiveness and flying flexibility, as they are not constrained by the physical structures of the power line conductors [5]. The MDR integrates the concept of power line health inspection with the damping properties of Aeolian vibration dampers [6]. By incorporating vibration control characteristics, the MDR eliminates the need for com-

plex climbing mechanisms over the dampers, while also enhancing vibration mitigation by approaching the nearest anti-node and adapting to changing wind conditions [7–10]. The design prototype of MDR is depicted in Fig. 3. The MDR will be equipped with a close-view camera positioned along the vertical line to face the top of the conductor. Finalizing this design consideration was crucial before data collection, ensuring that we captured images of the conductor according to our research plan.

FIGURE 3: Conceptual design model of the MDR.

3 ANALYSIS OF METHODS FOR DETECTING DEFECTS AND CORROSION

Image processing plays a crucial role in extracting desired details and suppressing background noise and unwanted surface features on a conductor. When working with cameras that capture colored (RGB) images, the first step is to convert these colored images into gray-scaled images. This conversion not only reduces computing time but also enhances the visibility against the background. The images of power line conductors often contain background noises, which decreases image quality and obscures important features. To optimize the identification of defects or corrosion and differentiate between healthy and unhealthy conductors, it is essential to effectively suppress any features that are not relevant to these details.

3.1 Sobel and Scharr Operator

Prior to integrating the Sobel and Scharr operator, the initial step involves applying Gaussian blur to the gray-scale image. Gaussian blur is a technique used to reduce noise in images by applying a Gaussian function that calculates the transformation for each pixel. This step is essential for noise reduction before applying Sobel and Scharr operators. The Gaussian filtering process can be represented by the convolution in the equation 1, where μ represents the mean (peak), and σ represents the variance of each x and y variable [11]. Figure 4 shows the images with a Gaussian filter applied to gray-scale images.

$$G_0(x,y) = A \cdot e^{-\frac{(x-\mu_x)^2}{2\sigma_x^2} - \frac{(y-\mu_y)^2}{2\sigma_y^2}} \tag{1}$$

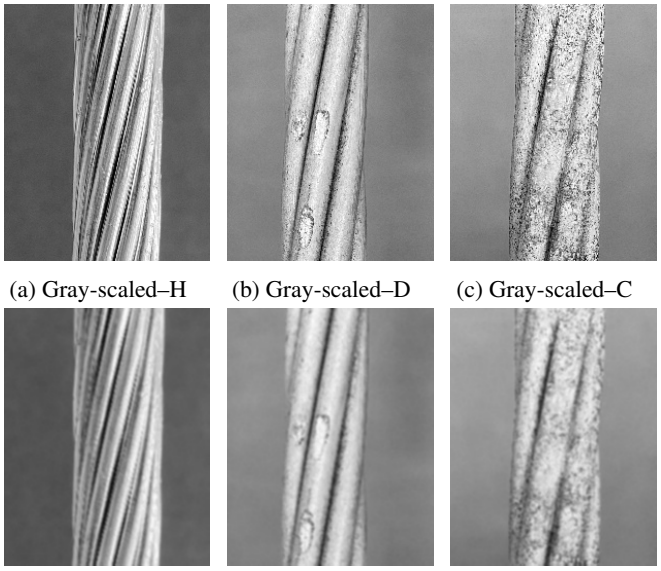

(a) Gray-scaled–H (b) Gray-scaled–D (c) Gray-scaled–C

(d) Blurred–H (e) Blurred–D (f) Blurred–C

FIGURE 4: Gray-scaled images and Gaussian blurred images (H: healthy, D: defect, C: corrosion).

Then, we employed the Sobel [12] and Scharr operators, both commonly used gradient-based edge detection techniques. One of the main distinctions between these operators is their approach to noise and weak edges. The Sobel operator excels at reducing background noise but may overlook weak edges that lack prominent features. On the other hand, the Scharr operator is more adept at detecting weak edges but may retain more noise in the process. Figure 5 illustrates the comparison of the first-order derivative weights of the Sobel and Scharr operators. The Sobel operator has weights of ± 1 and ± 2, while the Scharr operator has weights of ± 3 and ± 10. These weight differences demonstrate that the Scharr operator amplifies the influence of points with smaller gradient values, thereby retaining weaker edges. In our method, the operators convolve the image in horizontal and vertical directions to obtain gradient values of G_x and G_y. With those gradient values, gradient amplitude and gradient angle can be calculated with equations 2 and 3 [13]. The result of applying the Sobel and Scharr operators to the Gaussian-blurred gray-scale images is shown in Fig. 6. As the processed images demonstrate, the Scharr operator retains more weak edges compared to Sobel, which excels in noise reduction.

$$G = \sqrt{G_x^2 + G_y^2} \tag{2}$$

$$\theta = \arctan\left(\frac{G_y}{G_x}\right) \tag{3}$$

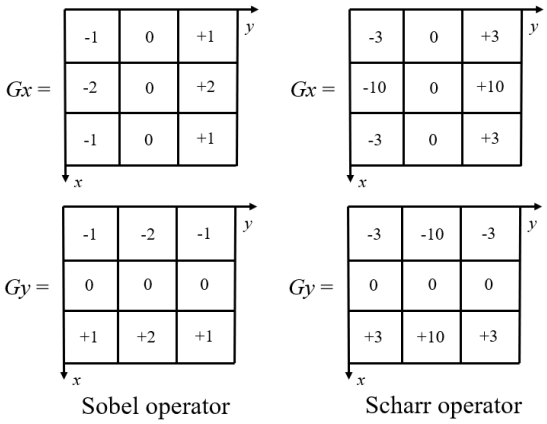

FIGURE 5: Sobel and Scharr convolution kernels

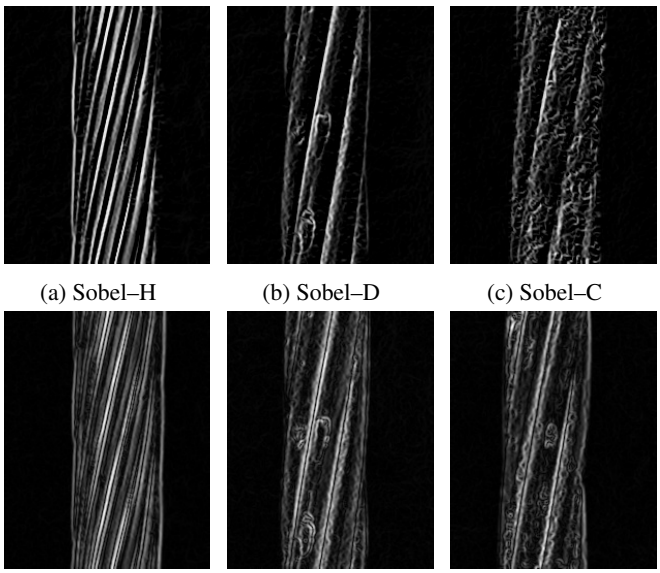

(a) Sobel–H (b) Sobel–D (c) Sobel–C

(d) Scharr–H (e) Scharr–D (f) Scharr–C

FIGURE 6: Results of image processing with Sobel or Scharr operators (H: healthy, D: defect, C: corrosion).

3.2 GVN

The GVN method aims to enhance the anti-background interface, clarity, and contrast within images, especially in regions with high-definition features like power line conductors compared to the background. This method differs from the traditional method by focusing on processing the dispersion degree of pixel gray values rather than directly processing the gray value of each pixel. In our implementation of the GVN algorithm, we first defined a template size of 3x3 pixels. This template is used to calculate the mean value. Next, the variance of the gray-scale value is computed within each unit of the template. The central pixel of the template adopts the mean of the calculated variance value, which highlights variations in intensity across the image. These iterative calculations are applied across the entire image using the 3x3 template, constructing a comprehensive gray-scale variance map. To further enhance the effectiveness of the GVN method, the gray-scale variance of each pixel is normalized using the equation 4:

$$m(x,y) = \frac{q(x,y) - q_{\min}}{q_{\max} - q_{\min}} \tag{4}$$

Here, $m(x,y)$ represents the normalized gray value at the pixel (x,y), $q(x,y)$ indicates the gray value at coordinate (x,y), q_{max} is the maximum gray value in the gray-scale variance map, and q_{min} is the minimum value of the variance map [14]. This normalization ensures consistency in the representation of intensity variations. The application of the GVN method to the gray-scale images is shown in Fig. 7. The images processed with the GVN method effectively highlight surface defects and corrosion while simultaneously suppressing background noise and unwanted surface details. This contrast is particularly noticeable when compared to images processed with Sobel and Scharr operators, which proves the superior performance of the GVN method in enhancing the visibility of critical features relevant to power line inspection.

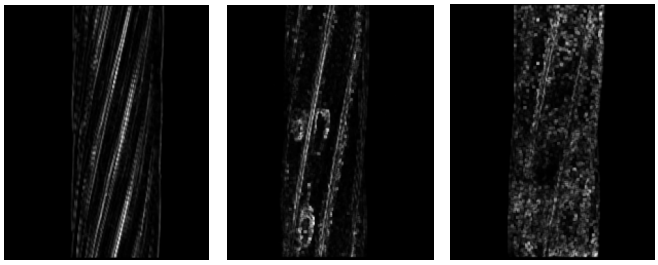

(a) Healthy (b) Defect (c) Corrosion

FIGURE 7: Results of image processing with GVN method.

3.3 Histogram Analysis

The Defect Localization Based on Projection Profile (DLBP) algorithm utilizes the distinct gray values of defects compared to the background. By examining the spatial clustering of defect patterns, which differs from the more uniformly distributed noise and background in the image, the algorithm calculates the mean of gray value along longitudinal and transverse projection [15]. In our implementation, we observed a similar pattern of the spatial clustered gray values in areas with defects and corrosion. By

calculating the mean gray values along both transverse and longitudinal directions, we derived histograms, providing a quantitative representation of the observed patterns. Figure 8 shows a GVN method processed image of a defective conductor. With a column and row analysis of mean gray values, both histograms portray peaks in the range of pixels where the area of defects contains clusters of higher gray values. In particular, row analysis showed an easily visible pattern of these abnormalities.

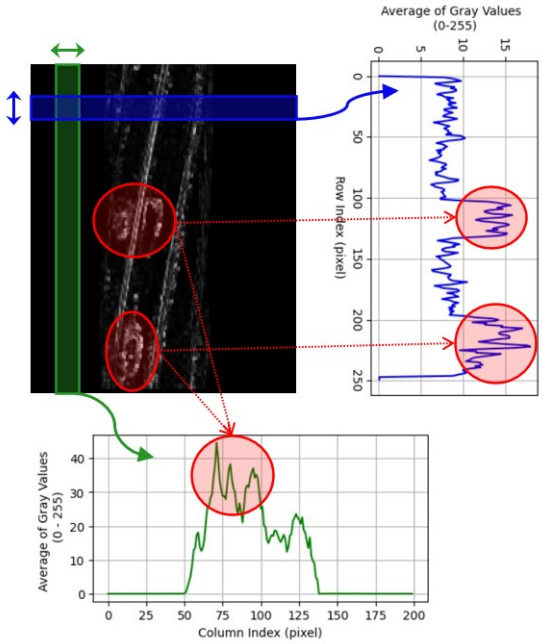

FIGURE 8: Histogram analysis of the processed image.

Figures 9 and 10 display the row and column histogram of images with healthy, defective, and corroded conductors processed using the GVN method. The row histogram analysis of the healthy conductor image shows a consistent gray value, with peaks that are not significantly different. In contrast, the row histograms of images with defective and corroded conductors show significant differences in peak values, effectively capturing the pattern of defects and corrosion. This analysis of histogram proved effective in distinguishing healthy conductors from those with defects or corrosion, highlighting its potential to capture more relevant features related to classification beyond just peak values. This aspect will be further discussed in the experiment section of the paper.

4 CLASSIFICATION WITH MACHINE LEARNING MODELS

Machine learning models were used to classify the conductors' condition (healthy, unhealthy) based on the gray-scale histogram. Since the models were trained using the labeled image dataset, supervised learning classification models were selected. Supervised learning classification models are trained on labeled data, allowing them to predict labels for new data based on the established relationship between the features of the data and their corresponding labels. Supervised learning classification models can be categorized based on their underlying algorithms [16–18], including logic-based algorithms, neural network algorithms, ensemble algorithms, and statistical learning algorithms. Since we conducted the classification using data collected on gray-scale images in pixel space with edge features, we selected models from each category: a logic-based algorithm (Random Forest model [18, 19]), a neural network algorithm (Multi-Layer Perception model [20, 21]), and an ensemble algorithm (Gradient Boosting model [22, 23]).

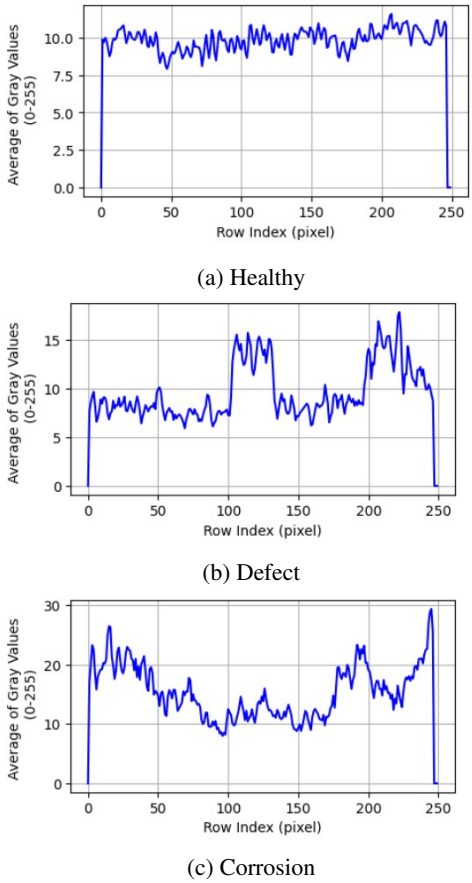

(a) Healthy

(b) Defect

(c) Corrosion

FIGURE 9: Histograms of rows from GVN method (healthy, defect, corrosion).

4.1 Random Forest

Random Forest (RF) is a combination of independent decision trees and uses averaging to improve predictions and control over

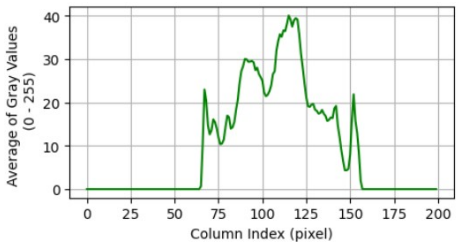

(a) Healthy

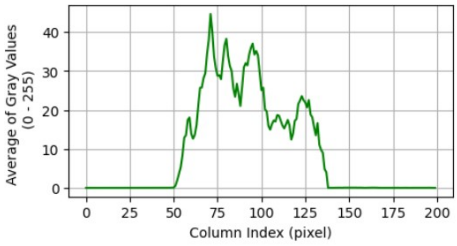

(b) Defect

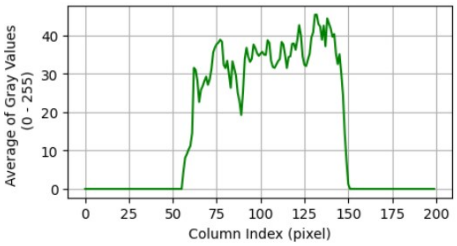

(c) Corrosion

FIGURE 10: Histograms of columns from GVN method (healthy, defect, corrosion).

fitting. Each tree relies on the values of a random vector sampled independently and with the same distribution for all trees in the forest [18]. RF predicts the class by considering the ensemble of trees, selecting the class that receives the most votes from the individual trees. The single tree average for prediction probability is

$$p_{RF}^{T_{\text{tree}}}(c_{RF}^{T_{\text{tree}}} \in \{M,I\} \mid Y) = \frac{1}{T_{\text{tree}}} \sum_{1}^{T_{\text{tree}}} P_{Sn(\theta n,T)}(c_n \in \{M,I\} \mid Y) \tag{5}$$

where $p_{RF}^{T_{\text{tree}}}(c_{RF}^{T_{\text{tree}}} \in \{M,I\} \mid Y)$ is probability p conditioned on the event c occurring over T_{tree}, where c is a variable representing the condition $(\{M,I\} \mid Y)$. $P_{Sn}(\theta n,T)$ is the probability associated with Y by the RF tree statistical model $Sn(Y,\theta n)$. RF effectively captures complex interactions and reduces combination-based variance through collaborative work among multiple trees.

4.2 Multi-Layer Perceptron

Multi-Layer Perception (MLP) is a feed-forward artificial neural network model used for classification. It comprises multiple layers of neurons, including an input layer, one or more hidden layers, and an output layer. Each neuron in the network is connected to every neuron in the subsequent layer, with associated weight on each connection. MLP utilizes the backpropagation technique for supervised learning, updating weights as described in equation 6 [21]. Here, η represents the learning rate, δ_j is the error related with neuron j, and O_i is the output computed by neuron i. This learning structure enables MLP to discern complex patterns in data that are not linearly separable, making it effective for handling intricate classification tasks.

$$\Delta W_{ji} = \eta \delta_j O_i \tag{6}$$

4.3 Gradient Boosting

Gradient Boosting (GB) is a machine learning technique that sequentially fits new models to improve predictions about the response variable. It works by minimizing errors from previous models through an ensemble function estimate defined by equation 7 [22].

$$(\rho_t, \theta_t) = \arg\min_{\rho,\theta} \sum_{i=1}^{N} [-g_t(x_i) + \rho h(x_i,\theta)]^2 \tag{7}$$

Here, ρ_t represents the best gradient descent step-size, θ_t is the estimate, $g_t(x_i)$ is the negative gradient, ρ is the optimal step-size, and $h(x_i,\theta)$ is a new base-learner function. Each new model aims to be highly correlated with the negative gradient of the loss function associated with the entire ensemble of models. GB offers flexibility in the selecting the loss function, making it customizable for specific data-driven tasks. Moreover, it is relatively simple to implement, allowing experimentation with various model designs.

5 EXPERIMENTS

To collect the images of healthy and unhealthy power line conductors, we obtained new and aged conductors from industry sources. New power line conductors were ordered to capture images of healthy lines from desired angles and positions. The electric companies supplied aged, obsolete conductors that had defects and corrosion and were no longer in use. These collected images present an optimal representation for our experiment as the aged conductors naturally showcase corrosion and defects that occur over time. This approach ensures the practicality and real-world relevance of our defect and corrosion detection method. For the training dataset, we collected a total of 254

images of healthy conductors and 478 images of unhealthy conductors. The testing dataset comprised of 33 images of healthy conductors and 67 images of unhealthy conductors.

5.1 Feature Extraction

The gray-scale histograms were analyzed to extract features for classification. As shown in Fig. 11, we derived ten features, including the number of peaks, maximum, minimum, range, and average for each columns and rows. Only the dominant peaks were counted, and the range was calculated as the difference between the maximum and the minimum value, representing the lowest valley.

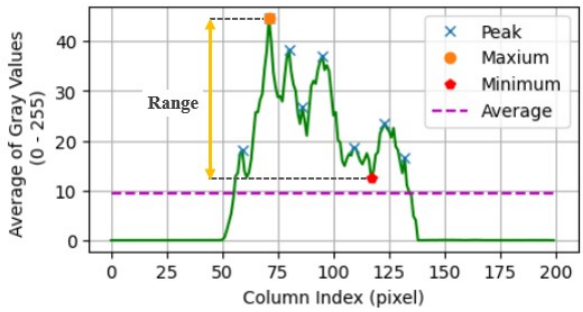

FIGURE 11: Feature extraction from histogram.

5.2 Model Selection

Three supervised classification models (RF, MLP, GB) for the Sobel, Scharr, and GVN methods were trained and classified using Scikit-learn software. Their performances were analyzed using metrices such as accuracy, F1 score, precision, and recall, as detailed in Table 1. Accuracy represents the proportion of correct predictions, precision measures accurate identification of negative samples, and recall assesses the model's ability to identify positive samples. The F1 score provides a balanced assessment of a model's performance and is derived from precision and recall using equation (8), where TP is the number of true positives, FP is the number of false positives, and FN is the number of false negatives. A value of 1 indicates optimal performance, while a value of 0 reflects the worst performance across all metrics.

$$F1 = \left(\frac{2 * TP}{2 * TP + FP + FN} \right) \tag{8}$$

In Table 1, the GVN method achieved superior performance with the MLP model, achieving an accuracy of 90%. The Scharr operator performed the best with the GB model, achieving an accuracy of 88%, while the Sobel operator, the lowest among the three, achieved an accuracy of 83% with the RF model.

TABLE 1: Results of experiments with full features.

	Model	Accuracy [%]	F1 [%]	Precision [%]	Recall [%]
Sobel	RF	83.00	83.27	81.82	71.05
	MLP	81.00	80.92	69.70	71.88
	GB	79.00	79.22	72.73	66.67
Scharr	RF	86.00	85.88	75.76	80.65
	MLP	83.00	82.93	72.73	75.00
	GB	88.00	87.90	78.79	83.87
GVN	RF	89.00	89.04	84.85	82.35
	MLP	90.00	90.13	90.91	81.08
	GB	85.00	85.15	81.82	75.00

5.3 Feature Selection

The complexity of a model increases exponentially with the number of features, raising the risk of overfitting. Irrelevant or redundant features can lead the model to learn specific training data patterns, hindering generalization to new data. Feature selection mitigates overfitting by prioritizing the most informative features significantly contributing to the model's predictive performance. Additionally, models trained on a reduced set of relevant features are generally more robust to noise and outliers in the data. Therefore, feature selection is crucial in enhancing the performance, efficiency, interpretability, and robustness of machine learning models [24, 25].

We performed feature selection for the Sobel, Scharr, and GVN methods with the best performance models for each. A feature selection technique provided by the scikit-learn (sklearn) library in Python, `SelectKBest`, was used with the `f_classif` scoring function. `SelectKBest` enables the selection of the top k-number of features from a dataset, considering their statistical significance concerning the target variable. As shown in Table 2, Sobel operator improved its accuracy by 1% when eight features (column maximum, column minimum, column range, column average, row number of peaks, row maximum, row minimum, and row average) were selected. The GVN method, which showed the best performance, achieved an accu-

TABLE 2: Results of experiments with selected features.

	Model	Accuracy [%]	F1 [%]	Precision [%]	Recall [%]
Sobel	RF ($k = 8$)	84.00	84.21	81.82	72.97
Scharr	GB ($k = 10$)	88.00	87.90	78.79	83.87
GVN	MLP ($k = 4$)	92.00	92.06	90.91	85.71

racy of 92%, with an increase of 2% when four features (column range, row number of peaks, row minimum, and row range) were selected. On the other hand, Scharr operator was confirmed to have the best performance for all 10 features.

6 RESULTS AND DISCUSSION

The table 3 displays the number of incorrect classifications made by each image processing technique paired with its best-performing machine learning model for healthy and unhealthy conductors. The error analysis shows that there is no discernible pattern in the ratio of incorrect classifications between healthy and unhealthy categories for each image processing technique. Specifically, while the GVN method misclassified an equal number of healthy and unhealthy conductors, the Sobel and Scharr operators misclassified different ratio of unhealthy and healthy conductors, respectively. This lack of pattern could be attributed to the characteristics of each image filtering method, and the varied use of features and classification models.

The GVN method produced the best performance overall but demonstrated a slightly lower accuracy for healthy data, given the 1:2 ratio of healthy to unhealthy data in the test dataset. Several explanations can be made for this result. Firstly, the training dataset for healthy conductors was smaller (254 images) compared to the dataset for unhealthy conductors (478 images). This discrepancy in dataset sizes could have made it more challenging for the machine learning model to accurately distinguish images with healthy conductors. Additionally, during the healthy conductor image collection, lower-quality images were obtained, such as uneven lighting and varying light reflectivity from different finishes of the metal surface. Since image processing techniques rely on image gradient calculations, they are highly sensitive to lighting conditions and reflectivity, which could have contributed to the higher number of incorrect classifications for healthy conductors. Thus, in the future, additional modifications to the images and exploring more methods to incorporate features are crucial for accurately classifying healthy conductors.

TABLE 3: Incorrect prediction analysis.

	Healthy [number]	**Unhealthy** [number]
Sobel	5	11
Scharr	7	5
GVN	4	4

7 CONCLUSION

This paper presents a method for classifying images of power line conductors as healthy or unhealthy, crucial for the MDR's health inspection system. Through image processing, row and column analysis, and supervised machine learning, the proposed method achieves accurate classification. Among image filtering techniques, the GVN method proved to be the most effective, and the MLP model with four features demonstrated the highest accuracy.

ACKNOWLEDGMENTS

This work is funded by National Science Foundation CAREER Award ECCS 1944032: Towards a Self-Powered Autonomous Robot for Intelligent Power Lines Vibration Control and Monitoring. Any opinions, findings, and conclusions or recommendations expressed in this material are those of the author(s) and do not necessarily reflect the views of the National Science Foundation.

REFERENCES

[1] Oumar Barry, Donatus CD Oguamanam, and Der Chyan Lin. Aeolian vibration of a single conductor with a stockbridge damper. *Proceedings of the Institution of Mechanical Engineers, Part C: Journal of Mechanical Engineering Science*, 227(5):935–945, 2013.

[2] Aamir Malik, Likun Xia, and Nadia Ashikin. Vegetation encroachment monitoring for transmission lines right-of-ways: A survey. *Electric Power Systems Research*, 95:339–352, 02 2013.

[3] Ludan Wang, Sheng Cheng, and Jianwei Zhang. Development of a line-walking mechanism for power transmission line inspection purpose. In *2009 IEEE/RSJ International Conference on Intelligent Robots and Systems*, pages 3323–3328, 2009.

[4] Ludan Wang, Sheng Cheng, and Jianwei Zhang. Development of a line-walking mechanism for power transmission line inspection purpose. In *2009 IEEE/RSJ International Conference on Intelligent Robots and Systems*, pages 3323–3328, 2009.

[5] Jiang Bian, Xiaolong Hui, Xiaoguang Zhao, and Min Tan. A novel monocular-based navigation approach for uav autonomous transmission-line inspection. In *2018 IEEE/RSJ International Conference on Intelligent Robots and Systems (IROS)*, pages 1–7, 2018.

[6] Oumar R. Barry, Emadeddin Y. Tanbour, Nitish K. Vaja, and Hesham Tanbour. Asymmetric aeolian vibration damper, April 17 2018. US Patent 9,948,081.

[7] Paul-Camille Kakou. *Towards A Mobile Damping Robot For Vibration Reduction of Power Lines*. PhD thesis, Virginia Tech, 2021.

[8] Paul Kakou, Mohammad Bukhari, Jiamin Wang, and Oumar Barry. On the vibration suppression of power lines using mobile damping robots. *Engineering Structures*, 239:112312, 2021.

[9] Andrew Choi and Oumar Barry. Testing and validation of a mobile damping robot for power lines. *International Design Engineering Technical Conferences and Computers and Information in Engineering Conference.*, 87400, 2023.

[10] Andrew Choi, Paul-Camille Kakou, and Oumar Barry. Considerations for the testing and validation of a mobile damping robot for overhead power lines. Volume 10: 34th Conference on Mechanical Vibration and Sound (VIB):V010T10A026, 08 2022.

[11] Gusti Ayu Almira, Tri Harsono, Riyanto Sigit, I. G. N. T. B. Bimantara, and J. S. Michael Saputra. Performance analysis of gaussian and bilateral filter in case of determination the fetal length. In *2016 International Conference on Knowledge Creation and Intelligent Computing (KCIC)*, pages 246–252, 2016.

[12] Jianfang Cao, Lichao Chen, Min Wang, and Yun Tian. Implenmenting a parallel image edge detection alogirthm based on the otsu-canny operator on the hadoop platform. *Computational Intelligence and Neuroscience*, 2018.

[13] Bingjun Weng, Wei Gao, Weicou Zheng, and Gengjie Yang. Newly designed identifying method for ice thickness on high-voltage transmission lines via machine vision. *High Voltage*, 6(5):904–922, 2021.

[14] Ye Zhang, Xinbo Huang, Jianyuan Jia, and Xinhui Liu. A recognition technology of transmission lines conductor break and surface damage based on aerial image. *IEEE Access*, 7:59022–59036, 2019.

[15] Qingyong Li and Shengwei Ren. A real-time visual inspection system for discrete surface defects of rail heads. *IEEE Transactions on Instrumentation and Measurement*, 61(8):2189–2199, 2012.

[16] Christopher M. Bishop and Nasser M. Nasrabadi. *Pattern recognition and machine learning.*, volume 4. New York: springer, 2006.

[17] Sotiris B. Kotsiantis, Ioannis Zaharakis, and P. Pintelas. Supervised machine learning: A review of classification techniques. *Emerging artificial intelligence applications in computer engineering*, 160.1:3–24, 2007.

[18] Debani P. Mishra and Papia Ray. Fault detection, location and classification of a transmission line. *Neural Computing and Applications*, 30:1377–1424, 2018.

[19] Leo. Breiman. Random forests. *Machine learning*, 45:5–32, 2001.

[20] Alexander Iversen, Nicholas K. Taylor, and Keith E. Brown. Classification and verification through the combination of the multi-layer perceptron and auto-association neural networks. *2005 IEEE International Joint Conference on Neural Networks*, 2, 2005.

[21] Shalin Savalia and Vahid Emamian. Cardiac arrhythmia classification by multi-layer perceptron and convolution neural networks. *Bioengineering*, 5.2(35), 2018.

[22] Alexey Natekin and Alois Knoll. Gradient boosting machines, a tutorial. *Frontiers in neurorobotics*, 7(27), 2013.

[23] Fabio Sigrist. Gradient and newton boosting for classification and regression. *Expert Systems With Applications*, 167(114080), 2021.

[24] Andreas Janecek, Wilfried Gansterer, Michael Demel, and Gerhard Ecker. On the relationship between feature selection and classification accuracy. *Workshop on New challenges for feature selection in data mining and knowledge discovery*, 4:90–105, 2008.

[25] Jiliang Tang, Salem Alelyani, and Huan Liu. Feature selection for classification: A review. *Data classification: Algorithms and applications*, (37), 2014.